Technical note: On the ice microphysics of isolated thunderstorms and non-thunderstorms in southern China: A radar polarimetric perspective

Chuanhong Zhao[*1,2], Yijun Zhang[*1,3], Dong Zheng[4], Haoran Li[4], Sai Du[5], Xueyan Peng[2], Xiantong Liu[5], Pengguo Zhao[2], Jiafeng Zheng[2], Juan Shi[6]

[1]*Department of Atmospheric and Oceanic Sciences & Institute of Atmospheric Sciences, Fudan University, Shanghai, China*

[2]*School of Atmospheric Sciences, Chengdu University of Information Technology, Chengdu, China*

[3]*Shanghai Key Laboratory of Ocean-land-atmosphere Boundary Dynamics and Climate Change & Shanghai Frontiers Science Center of Atmosphere-Ocean Interaction, Fudan University, Shanghai, China*

[4]*State Key Laboratory of Severe Weather, Chinese Academy of Meteorological Sciences & Laboratory of Lightning Physics and Protection Engineering, Chinese Academy of Meteorological Sciences, Beijing, China*

[5]*Guangzhou Institute of Tropical and Marine Meteorology, Guangzhou, China*

[6]*Chengdu Meteorological Office, Chengdu, China*

Corresponding authors: Dr. Yijun Zhang & Dr. Chuanhong Zhao are the co-corresponding authors.

E-mail: zhangyijun@fudan.edu.cn; zch@cuit.edu.cn

Abstract

Determining whether a cloud will evolve into a thunderstorm is beneficial for understanding thunderstorm formation and is also important for ensuring the safety of society. However, a clear understanding of the microphysics of clouds in terms of the occurrence of lightning activity has not been attained. Vast field observations and laboratory experiments indicate that graupel, which is rimed ice, is a vital hydrometeor for lightning generation, and is the foundation of riming electrification. In this study, polarimetric radar and lightning observations are used to compare the ice microphysics associated with graupel between 57 isolated thunderstorms and 39 isolated non-thunderstorms, and the differences in radar parameters are quantified. Our results for the occurrence of lightning activity in clouds revealed the following results: 1) the maximum difference in graupel volume at the −10°C isotherm height between thunderstorms and non-thunderstorms reached approximately 7.6 km^3; 2) the graupel particles approached spherical shapes with a mean differential reflectivity (Z_{DR}) value of 0.3 dB, which likely indicated that heavily rimed graupel was present; 3) the median values of horizontal reflectivity (Z_H) or Z_{DR} at positions where the source initiation and channel of the first lightning flashes were nearly 31 dBZ or 0 dB; and 4) 98.2% of the thunderstorms were equipped with a Z_{DR} column, and the mean depth was ~2.5 km. Our study deepens our understanding of lighting physics and thunderstorm formation.

Short summary

Understanding lightning activity is important for meteorology and atmospheric chemistry. However, the occurrence of lightning activity in clouds is uncertain. In this study, we quantified the difference between isolated thunderstorms and non-thunderstorms. We showed that lightning activity was more likely to occur with more graupel volume and/or riming. A deeper Z_{DR} column was associated with lightning occurrence. This information can aid in a deeper understanding of lighting physics.

Keywords: thunderstorm; lightning; riming; cloud microphysics

1. Introduction

Thunderstorms are typically severe convection clouds. Lightning is not only a severe weather hazard produced by thunderstorms but also a clear signature of thunderstorm formation (MacGorman and Rust, 1998). Understanding lightning activity (especially for the first lightning flash, which indicates the start of lightning activity in a cloud) is important for understanding meteorological processes and the formation of thunderstorms (Uman and Krider, 1989; Rosenfeld et al., 2008; Fan et al., 2018) and for investigating related atmospheric chemistry, such as the formation of ozone and the primary oxidant in the troposphere, the hydroxyl radical (Pickering et al., 2016; Brune et al., 2021).

The determination of whether a cloud will evolve into a thunderstorm is very difficult. The occurrence of lightning activity in clouds is a complex process involving dynamics, microphysics and electrical processes (e.g., Krehbiel et al., 1979; MacGorman and Rust, 1998; Carey and Rutledge, 2000; Stolzenburg et al., 2001; Saunders, 2008; Zhang et al., 2009; Lang and Rutledge, 2011; Zhang et al., 2016; Stough and Carey, 2020; Lyu et al., 2023). Moreover, natural lightning flashes can be categorized as intracloud lightning and cloud-to-ground lightning (Uman and Krider, 1989). Some studies have indicated that the majority of the first lightning flashes are intracloud lightning, which was concluded from the statistical results observed by polarimetric radar and lightning location systems (e.g., Mattos et al., 2017; Zhao et al., 2021a). In addition, there is a generally accepted electrification cause, especially for clarifying the first lightning flash occurrence correctly: noninductive charging (NIC) of two ice particles of different sizes during rebounding collisions in the presence of supercooled droplets, with the smaller ice particle being the ice crystal and the larger ice particle being the graupel(Takahashi, 1978; Latham, 1981; Saunders et al., 1991; MacGorman and Rust, 1998; Carey and Rutledge, 2000; Zhang et al., 2009; Takahashi et al., 2017, 2019; Qie et al., 2021; Lyu et al., 2023).

The NIC was proposed on the basis of cold-chamber laboratory experiments (Reynolds et al., 1957; Takahashi, 1978). Subsequently, field observations demonstrated that lightning production is critically linked to ice processes (i.e., graupel signatures) (Dye et al., 1986; Takahashi et al., 1999; Carey and Rutledge, 2000; Basarab et al., 2015; Stolzenburg et al., 2015; Mattos et al., 2016, 2017; Takahashi et al., 2017, 2019; Hayashi et al., 2021; Zhao et al., 2022). Numerical simulation

studies also support the NIC mechanism as the main contributor to charge separation conducive to lightning flash triggering at timescales relevant to storm duration (e.g., Helsdon et al., 2001; Mansell et al., 2005; Barthe and Pinty, 2007). Therefore, graupel is a vital precipitation particle for riming electrification mechanism.

Graupel is rimed precipitation ice. However, the mechanisms for graupel formation vary with cloud type. One pathway to graupel that is very common in warm based clouds worldwide is the development of rain drops in warm rain collision-coalescence processes (e.g., Brahams, 1986; Beard, 1992; Herzegh and Jameson, 1992; Bringi et al., 1997; Carey and Rutledge, 2000), followed by lofting of the rain drop in the updraft to subfreezing temperatures (which is frequently observed by polarimetric radar, called the differential reflectivity (Z_{DR}) column), then by drop freezing and finally riming into graupel or small hail. This coalescence-freezing mechanism is often the most important pathway to the first graupel/hail, the first significant electrification and the first lightning flash in warm based clouds (e.g., Brahams, 1986; Beard, 1992; Herzegh and Jameson, 1992; Bringi et al., 1997; Smith et al., 1999; Carey and Rutledge, 2000; Stolzenburg et al., 2015; Mattos et al., 2017). Another pathway to graupel or small hail production is initiated via the aggregation of ice crystals into snow aggregates, followed by riming of the snow aggregate into graupel and possibly even small hail as the rime density increases (Heymsfield, 1982; Li et al., 2018).

It should also be emphasized that the formation of graupel is closely related to not only lightning activity but also the strength of updrafts in clouds, and the latent heat of freezing enhances updrafts, promoting severe storm formation (Rosenfeld, 1999; Zhang et al., 2004; Rosenfeld et al., 2008). More droplets freeze aloft and release more latent heat for nucleation, thereby invigorating convective updrafts and producing lightning, and deep convective clouds form (Rosenfeld, 1999; Zhang et al., 2004; Rosenfeld et al., 2008). Therefore, investigating the ice microphysics associated with graupel is essential for understanding thunderstorm formation.

Polarimetric radar is the best observation system for tracking the specific location and timing of a cloud and inferring the microphysical characteristics within clouds (e.g., Seliga and Bringi, 1976; Zrnic and Ryzhkov, 1999; Kumjian, 2013; Hu et al., 2019; Huang et al., 2023). Many studies (e.g., Laksen and Stansbury, 1974; Marshall and Radhakant, 1978; Dye et al., 1986;

Vincent et al., 2003; Latham et al., 2007; Woodard et al., 2012; Mattos et al., 2016, 2017; Hayashi et al., 2021; Zhao et al., 2022) have investigated the relationship between ice microphysics and lightning activity and provided methods for predicting the first lightning flash occurrence based on the riming electrification mechanism; specifically, graupel-related reflectivity at −10°C or colder is a commonly supported leading reflectivity parameter for forecasting the first lightning flash (e.g., Laksen and Stansbury, 1974; Marshall and Radhakant, 1978; Vincent et al., 2003; Woodard et al., 2012; Hayashi et al., 2021). However, the performances of these methods vary with season, geography, or other atmospheric variables; more directly, different ice microphysics within different clouds dominate. There is no doubt that the graupel signatures inferred by polarimetric radar are universally present in convective clouds, whereas some clouds involve no lightning (e.g., Woodard et al., 2012; Hayashi et al., 2021; Cui et al., 2022; Zhao et al., 2022). Specifically, the graupel signature inferred by the polarimetric radar needs to be partitioned into more details according to the radar parameters. Therefore, we conducted this study to better understand the ice microphysics associated with graupel within thunderstorms.

We accomplished this goal by comparing the ice microphysics associated with graupel between isolated thunderstorms and non-thunderstorms during the warm season over southern China and quantifying differences in graupel magnitude and shape (implying the riming efficiency) in radar parameters, instead of studying the evolution variation within the same thunderstorm (the role of some polarimetric signatures would be covered in the same cloud evolution). Furthermore, we discussed the possible microphysics associated with the source initiation and channel of the first lightning flash via 3D lightning mapping. To our knowledge, no other study addressing this topic has been published. In addition, we explored the role of the coalescence-freezing mechanism in the production of lightning based on the information provided by the Z_{DR} column, a narrow vertical extension of positive Z_{DR} values above the 0°C isothermal height associated with updrafts and supercooled liquid water in deep moist convective storms (e.g., Hall et al., 1980; Ryzhkov et al., 1994; Kumjian and Ryzhkov, 2008; Kumjian, 2013; Kumjian et al., 2014; Snyder et al., 2015; Zhao et al., 2020; Chen et al., 2023). Isolated thunderstorms are common in southern China during the warm season (Mai and Du, 2022). From the perspective of isolated storms in the warm season, the physical processes within clouds are easier to explain, and the characteristics of graupel

141 microphysics can be compared with those of cold-based clouds (Li et al., 2018).

142 **2. Materials and methods**

143 The dataset used in this study was the same as that used in Zhao et al. (2021a, 2022). In Zhao
144 et al. (2021a), the dataset was first shown to the public. They obtained observations of 57 (39)
145 isolated thunderstorms (non-thunderstorms) that occurred over South China in the warm season
146 (from late May to early September) of 2016 and 2017 from the S-band polarimetric radar and
147 three independent lightning location systems. The role of turbulence characteristics in producing
148 the first lightning flashes was evaluated on the basis of the dataset, and the results indicated that
149 the eddy dissipation rate of non-thunderstorms was clearly lower than that of thunderstorms (Zhao
150 et al., 2021a). Moreover, the polarimetric radar parameters of the first radar echoes (the first radar
151 volume scan when clouds are detected by radar) were compared to determine the early difference
152 between thunderstorms and non-thunderstorms on the basis of this dataset (Zhao et al., 2022). The
153 greater echo intensity occurred in non-thunderstorms below the −10°C isotherm height, and the
154 cause for this feature and effect on subsequent cloud development were simply discussed by
155 integrating comprehensive observations (e.g., the ERA-Interim reanalysis data, surface aerosol
156 concentration, and graupel and rainwater contents derived from radar observations).

157 The error in the graupel content estimated in Zhao et al. (2022) is uncertain, and the
158 efficiency of the microphysical process (i.e., riming) associated with graupel is unknown; this
159 represents a gap in understanding the role of graupel in the first lightning flash occurrence based
160 on field observations. Naturally, we aimed to identify a method to quantify differences in graupel
161 magnitude and riming efficiency in this study to minimize the error as much as possible. The radar
162 sample volume, which corresponds to graupel identification, was used to indicate the graupel
163 magnitude instead of the derived graupel content, as in Carey and Rutledge (2000) and Zhao et al.
164 (2022). The variety of Z_{DR} shapes was used to determine the riming efficiency. Thus, the goal and
165 method of this study were substantially different from those of the two previous studies noted
166 above, although they are based on the same dataset.

167 The Guangzhou S-band polarimetric radar (GZ radar) provided the radar data as marked by
168 the orange star in Figure 1. The beam width of the GZ radar was ≤1°, and a full radar volume scan

lasted 6 minutes; this consisted of nine elevation angles with a radial resolution of 250 m. A quality control procedure was carried out to remove ground clutter, anomalous propagation, and biological scatter, and the Z_{DR} offset of the raw data was corrected (Zhao et al., 2022). The quality-controlled radar data were interpolated onto a Cartesian grid at a horizontal resolution of 250 m and a vertical resolution of 500 m from 0.5 to 20 km above the mean sea level via nearest neighbour and vertical linear interpolation.

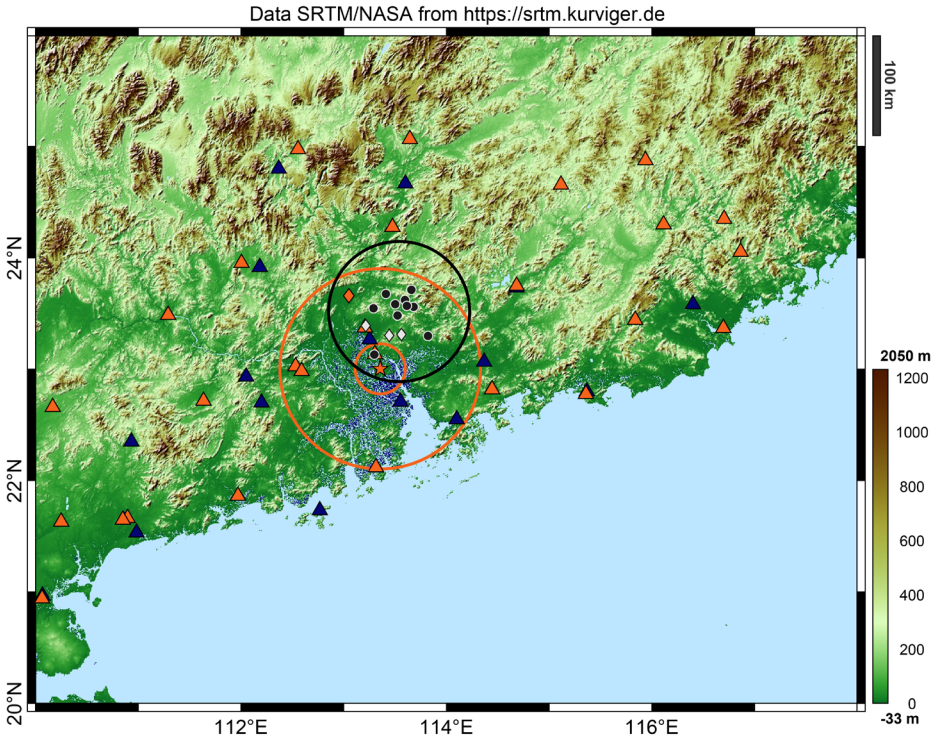

Figure 1. The locations of the detection systems and the analysed area. The orange star indicates the Guangzhou S-band polarimetric radar (GZ radar); the orange circles represent distances from the GZ radar site of 25 and 100 km. The black dots indicate the 10 sensors of the Low-Frequency E-field Detection array (LFEDA); the black circle indicates a distance of 70 km from the centre of the LFEDA network. The blue triangles indicate the 16 sensors of the Earth Networks Lightning Location System (ENLLS), and the orange triangles indicate the 27 sensors of the Guangdong Lightning Location System (GDLLS). The white diamonds indicate the three ground sites of aerosol concentration measurements. The orange diamond indicates the Qingyuan meteorological observatory. The analysed area is restricted to the regions of overlapping coverage between the GZ radar radius of 25−100 km and the LFEDA station network centre radius of 70 km.

A hydrometeor identification method, which is based on the fuzzy logic algorithm, was carried out to discriminate the graupel particles, as in Zhao et al. (2021b). The algorithm and approximate ranges of the S-band values of each polarimetric variable essentially followed Park et

al. (2009) and Kumjian (2013), with an improvement in the parameters of the membership functions of the fuzzy logic algorithm for the performance of the GZ radar, especially for dry/wet snow particles (Wu et al., 2018). In addition, temperature information was one of the few factors added to the hydrometeor identification method because it can separate liquid precipitation from solid hydrometeors to avoid visible identification errors (e.g., Bechini and Chandrasekar, 2015; Kouketsu et al., 2015; Zhao et al., 2020).

Three independent lightning location systems provided lightning observations. The low-frequency E-field detection array (LFEDA, as marked by black dots in Figure 1) can detect three-dimensional structures of intracloud lightning and/or cloud-to-ground lightning. The detection efficiency and mean location error of LFEDA for triggered lightning were approximately 100% and 102 m, respectively (Shi et al., 2017; Fan et al., 2018). The Earth Networks Lightning Location System (ENLLS, as marked by blue triangles in Figure 1) can detect two-dimensional locations for intracloud lightning and/or cloud-to-ground lightning. The detection efficiency and mean location error of ENLLS for triggered lightning and the natural strike of tall structure lightning were approximately 77% and 685 m, respectively (Zheng et al., 2017). The Guangdong Lightning Location System (GDLLS, as marked by orange triangles in Figure 1) can locate cloud-to-ground lightning. The detection efficiency and mean location error of the GDLLS for triggered lightning and the natural strike of tall structure lightning were approximately 94% and 741 m, respectively (Chen et al., 2012).

The lightning flash was assigned to its corresponding cell by using the boundary of the cell as a constraint every 6 minutes. The first lightning flash of a thunderstorm was defined by its first detection from one of three lightning location systems. An isolated non-thunderstorm cell was selected when no flash in the cell was detected by any of the three lightning location systems. To ensure detection-data quality, the analysis area was restricted to the regions of overlapping coverage between the GZ radar radius of 25–100 km and the LFEDA station network centre radius of 70 km (Figure 1), as in Zhao et al. (2021a, 2022). Any isolated cell storm generated within the analysis area that moved completely outside the analysis area or merged with other precipitation cells was excluded. The intersection of the 20 dBZ contours of the two intersecting cells is referred to as merging. For thunderstorms, we ensure that the first lightning flash of the cell must

occur before merging or when there is no merging. For storm cell development, if no merging process occurs and the maximum reflectivity of this cell starts to fade with a value of less than 30 dBZ later, the evolutionary process of a cell will mark the cessation stage. Our objective was to focus on isolated storm cells; therefore, if the merging process occurs before the fading of the maximum reflectivity of this cell, the evolutionary process of the cell will also signal the cessation stage.

In the dataset, six merging events occurred in non-thunderstorms, and the values of maximum reflectivity for these non-thunderstorms did not increase after merging occurred. In addition, the maximum reflectivity within any non-thunderstorm cell from initiation to cessation must exceed 45 dBZ to avoid the statistics of weak precipitation cells. Non-thunderstorms are characterized by no flash occurrence from initiation to cessation. The sounding data were obtained from the Qingyuan meteorological observatory, as marked by the orange diamond in Figure 1, which also provided the environmental temperature. Isolated thunderstorm/non-thunderstorm cells were identified and tracked manually based on the observations from the GZ radar and lightning location systems. The average distances between these storms and the radar/sounding site were approximately 70 and 56 km, respectively. More details related to these data and the selection methods for isolated thunderstorm and non-thunderstorm cells are available in Zhao et al. (2021a, 2022).

In this study, the evolution cycle of a thunderstorm consists of three stages: (i) the first radar volume scanning in cases where the horizontal reflectivity (Z_H) ≥ 5 dBZ is called the first stage (hereafter referred to as the #1 stage), (ii) the intermediate radar volume scanning between the first stage and the third stage is called the second stage (hereafter referred to as the #2 stage), and (iii) the radar volume scanning in cases where the first lightning flash occurs is called the third stage (hereafter referred to as the #3 stage). Similarly, the evolution cycle of a non-thunderstorm also contains three stages, but radar volume scanning in cases where the most intense echo occurs is called the third stage; here, the most intense echo is used to indicate the strongest convection development stage of non-thunderstorms for comparison with the first lightning flash stage of thunderstorms. The average durations from the first stage to the third stage for thunderstorms and non-thunderstorms were 19 and 24 minutes, respectively.

The majority of first lightning flash events (~98%) were considered intracloud flashes (IC flashes), and only one was considered a cloud-to-ground flash (CG flash) (Figure 2a). The majority of first lightning flashes (~91%) was determined by the LFEDA because of its superior detection efficiency and accuracy for detecting lightning flashes in this analysis area (Figure 2a). The elapsed time between the first radar volume scan and the first IC or CG flash (indicated by the first IC or CG return stroke) is shown in Figure 2b. The results show that the average elapsed time between the first radar volume scan and the first IC flash was approximately 19 minutes, and the first CG flash was approximately 32 minutes (Figure 2b). A recent study (Mattos et al., 2017) also revealed that in ~98% of thunderstorms, the first IC flash preceded the first CG flash, and the IC flashes occurred approximately 29 minutes after the first radar echo, CG flashes were most frequently delayed by approximately 36 minutes. The definition of the first radar echo may be the possible reason that the first flashes occurring after the first radar echo in Mattos et al. (2017) occurred later than those in our study.

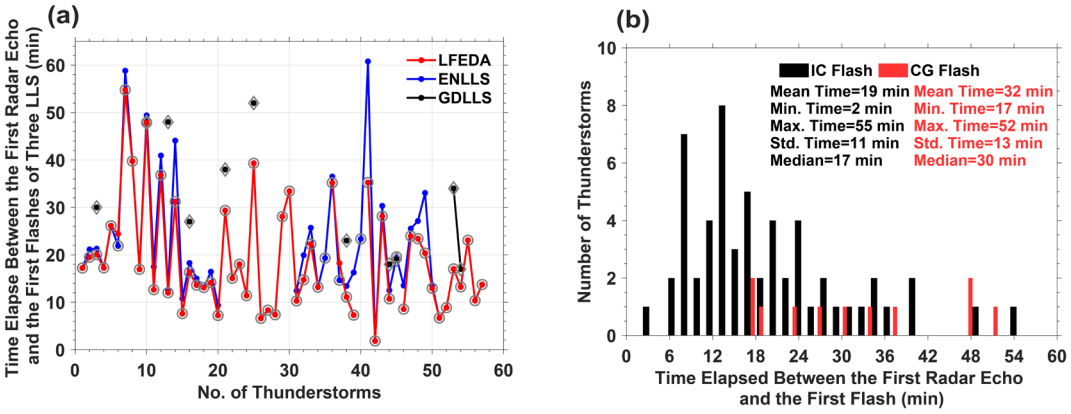

Figure 2. Lightning observations. Elapsed time between the first radar volume scan and (a) the first flashes of three lightning location systems, LFEDA (red line), ENLLS (blue line), and GDLLS (black line), where the grey circles indicate the first IC flashes, the grey diamonds indicate the first CG flashes, and (b) the elapsed time between the first radar volume scan and the first flashes of thunderstorms, the first IC flashes (black columns), and the first CG flashes (red columns).

In addition, the average 1-hourly surface concentration observations of particulate matter ($PM_{2.5/10}$) were provided by three ground sites (Figure 1, white diamonds) within the analysed area. The $PM_{2.5/10}$ concentration data suggest that the environment prior to these isolated thunderstorms or non-thunderstorms was clean and that the difference in the environmental aerosol concentration between thunderstorms and non-thunderstorms may be small (the mean values of $PM_{2.5/10}$ concentrations prior to thunderstorms and non-thunderstorms were 22.9/42 μg m^{-3} and 20.5/38.8

272 μg m^{-3}, respectively).

273 **3. Results**

274 **3.1 Morphology and intensity of the echoes in and/or before the first lightning flash**
275 **occurrence**

276 The scatters and triangles with error bars in Figure 3a depict the echo-top heights and
277 echo-base heights of the 57 thunderstorms and 39 non-thunderstorms from the first stage to the
278 third stage of cloud development via the reflectivity threshold (0 dBZ), and the echo depths are
279 shown in the box plots. The echo-top heights of thunderstorms and non-thunderstorms increase as
280 clouds develop. For the echo-top height data, approximately 95% of the thunderstorms exceeded
281 the −30°C isotherm height, and 85% exceeded the −38°C isotherm height of the glaciated layer
282 during the third stage of cloud development; however, only 26% and 23% of the
283 non-thunderstorms exceeded the −30°C and the −38°C isotherm heights, respectively, during the
284 third stage of cloud development. However, the echo-base heights mildly decreased with the
285 development of clouds; slight differences in the echo-base heights occurred between
286 thunderstorms and non-thunderstorms.

287 When the first lightning flashes occurred, approximately 84% of the thunderstorms and only
288 23% of the non-thunderstorms achieved an echo depth of 10 km. Lightning is the product of the
289 severe storms, and scientists often equate storm intensity with lightning flashes (e.g., Zipser et al.,
290 2006; Fan et al., 2018), but defining convective intensity is not as easy as it may seem (Zipser et
291 al., 2006); this could provide supplementary quantitative evidence for assisting scientists in
292 equating storm intensity with lightning flashes and determining the cloud depth corresponding to
293 the first lightning flash occurrence.

294 Figure 3b shows that the differences in the mean (maximum) values of the Z_H between the
295 thunderstorm and non-thunderstorm periods during each stage are slight; specifically, the median
296 differences in the mean values are −2, 2, and 3 dBZ, respectively. The median differences in the
297 maximum values are −4, 5, and 5 dBZ, respectively. Thunderstorms exhibit greater Z_H intensities
298 than non-thunderstorms do, except for those in the first stage of cloud development. The signature
299 of larger mean or maximum values of Z_H in non-thunderstorms during the first stage than in

thunderstorms has been discussed by Zhao et al. (2022), and this aspect is not the focus of this study. The mean or maximum values of Z_H in thunderstorms increase and exceed those in non-thunderstorms when the first lightning flashes occur; however, the box plots show that we cannot effectively differentiate thunderstorms from non-thunderstorms with respect to the Z_H intensity.

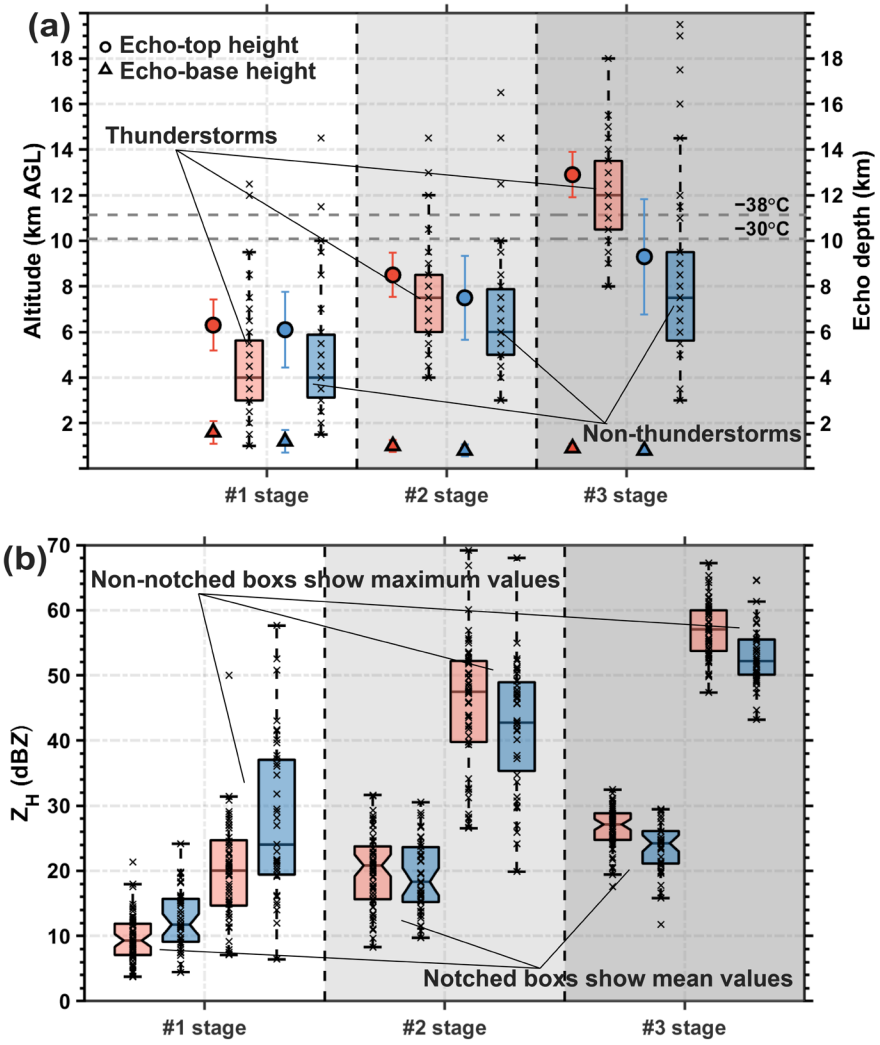

Figure 3. Characteristics of radar echoes with cloud development. (a) Echo-top heights of 0 dBZ and echo-base heights of 0 dBZ for 57 thunderstorm and 39 non-thunderstorm cells from the first stage to the third stage of cloud development are indicated by scatter points and triangles, respectively, with error bars. Error bars are computed as 95% confidence intervals. Box plots for the 57 thunderstorms (orange) and 39 non-thunderstorms (blue) for echo depths; all units are in km. The dashed grey lines indicate the −38°C and −30°C isotherm heights. (b) The mean (maximum) value of the Z_H in a thunderstorm or a non-thunderstorm during every stage is shown in notched box plots (non-notched box plots), with all units in the dBZ. The median values in the box plots are shown as black horizontal continuous lines. The temperature data were obtained from the sounding data of the Qingyuan

meteorological observatory.

3.2 Variations in graupel magnitude with cloud development

Graupel is a vital precipitation particle for the riming electrification mechanism, and its radar signature is not obscured by small ice particles. Thus, to investigate the microphysical characteristics related to the first lightning flash occurrence during storms, we obtained inferred "graupel", which was derived from the fuzzy-logic method based on the GZ radar (Park et al., 2009; Kumjian, 2013; Zhao et al., 2021b, 2022).

Each bar in Figure 4 indicates the mean value of the graupel volume in a height layer (the definition of the height layer is a vertical resolution of 500 m over 0.5 to 20 km above the mean sea level, 40 height layers in total) for 57 thunderstorms or 39 non-thunderstorms during each stage of cloud development. Specifically, the volume is computed by accumulating the radar sample grids; each radar sample grid is 0.03125 km^3, 0.25 km×0.25 km×0.5 km.

Graupel is rare in thunderstorms or non-thunderstorms during the first stage of cloud development (e.g., Dye et al., 1986; Mattos et al., 2017), and only 5% (13%) of thunderstorms (non-thunderstorms) show graupel signals (Figure 4). This finding is consistent with the results of Lang and Rutledge (2011), who indicated that the existence of a 30 dBZ echo above the freezing altitude is a necessary condition (in ~90% of cases) for lightning occurrence. This value is well above the 5 dBZ threshold used in this study to detect the first stage of a storm and can explain why graupel is rare in this stage. Moreover, in a modelling study of an isolated thunderstorm, Barthe and Pinty (2007) reported a delay of ~20 minutes between the first occurrence of graupel and the first lightning flash. In this case study, this delay was attributed to the time for graupel and vapour-grown ice to locally gain charge through the NIC mechanism and to the sedimentation of the different particles leading to macroscopic charge separation.

We proposed a mechanism for explaining the larger graupel volume in non-thunderstorms during the first stage of cloud development: more warm precipitation growth in non-thunderstorms due to cyclic drop growth resulting from coalescence under weaker updrafts may promote greater drop formation (Kumjian et al., 2014; Mather et al., 1986; Stough et al., 2021). These larger drops are lifted above the 0°C isothermal height and freeze to graupel-sized particles via a

coalescence-freezing mechanism (e.g., Bringi et al., 1997; Carey and Rutledge, 2000). With the development of clouds, that proportion of thunderstorms (non-thunderstorms) that produced graupel reaches 79% (51%) and 100% (95%) during the second and third stages of cloud development, respectively.

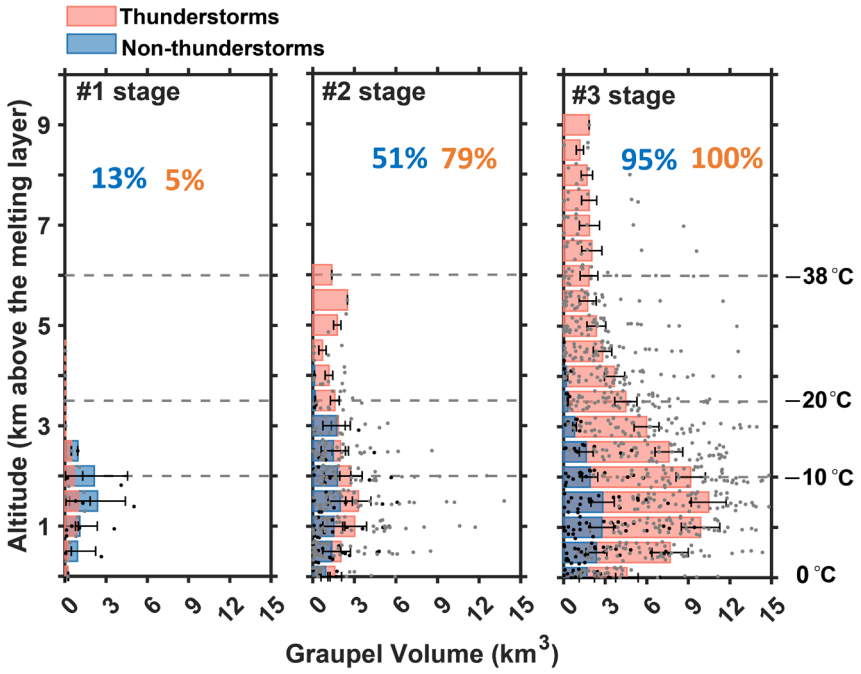

Figure 4. Distribution of graupel signals and volume with cloud development. Histogram plots with error bars for the distribution of the graupel volume above the melting layer for thunderstorm and non-thunderstorm cells during each stage of cloud development. Each grey dot indicates the total graupel volume on a height layer (the definition of the height layer is a vertical resolution of 500 m over 0.5 to 20 km above the mean sea level, 40 height layers in total) of a thunderstorm; the black dots indicate non-thunderstorms (units in km^3). The mean graupel volume in a height layer for the 57 thunderstorms is displayed as an orange histogram and a blue histogram shows the graupel volume for non-thunderstorm (in km^3). Error bars are computed as 95% confidence intervals. The numerical values in orange and blue are the percentages of thunderstorms and non-thunderstorms that show graupel signals, respectively. The left column represents the first stage of cloud development, and the right and middle rows represent the third and second stages of cloud development, respectively. The −10°C, −20°C, and −38°C isotherm heights are displayed in the histogram plots.

The greatest difference in graupel magnitude between thunderstorms and non-thunderstorms is found during the third stage of cloud development; the maximum difference in graupel volume in a height layer reaches approximately 7.6 km^3, and the height of the maximum difference is near the −10°C isotherm height. This information is consistent with the NIC electrification mechanism; namely, more graupel leads to more cloud electrification. In addition, more graupel corresponds to

more latent heat being released for convection invigoration. Interestingly, that the height corresponding to maximum difference of graupel volume is consistent with the main negative charge layer in thunderstorms over Guangzhou (Liu et al., 2020). Thus, the results suggested that the location of the negative charge layer may depend on the height of the maximum graupel magnitude. Notably, the graupel volume should be more accurately phrased as the presence of graupel in this volume. These characteristics indicate that graupel signals are universally present in thunderstorms and non-thunderstorms and that the difference in the magnitude of the graupel volume is the key for the first lightning flash occurrence.

3.3 More microphysical information based on radar variables

As the graupel volume increases from the first radar track to the occurrence of the first lightning flash, the graupel volume in thunderstorms is clearly greater than that in non-thunderstorms during the third stage of cloud development. However, the understanding of the details of the increase in graupel volume is limited (e.g., the variation in the maximum dimension or number concentration and precursor signature). In addition, although the coalescence-freezing mechanism dominating the formation of graupel within warm-season thunderstorms is generally accepted (e.g., Brahams, 1986; Beard, 1992; Herzegh and Jameson, 1992; Bringi et al., 1997; Smith et al., 1999; Carey and Rutledge, 2000; Stolzenburg et al., 2015; Mattos et al., 2017), more studies are needed to support this mechanism.

The Z_{DR} parameter could provide more information on graupel (e.g., shape) (e.g., Mattos et al., 2017; Li et al., 2018) and supercooled liquid water (e.g., Z_{DR} column) (e.g., Kumjian, 2013; Kumjian et al., 2014). The variance in the shape of the graupel indicates the riming efficiency; specifically, the heavily rimed ice particles approach a spherical shape (Kumjian, 2013; Li et al., 2018). Although the shape cannot directly indicate the variation in the maximum dimension, the speculated riming efficiency from the variation in the graupel shape could provide related information on the maximum dimension of graupel particles; typically, a more spherical shape (a decrease in Z_{DR}) and more riming result in a stronger Z_H corresponding to a larger maximum dimension (Li et al., 2018). The supercooled liquid water indicated by positive Z_{DR} values above the 0°C isothermal height is the precursor for freezing particles, followed by the embryo of graupel particles (e.g., Carey and Rutledge, 2000). Thus, the existence and/or variance of the Z_{DR}

column before the occurrence of the first lighting flash could support the coalescence-freezing mechanism. Moreover, we can obtain the quantitative difference in the Z_{DR} between thunderstorms and non-thunderstorms, especially for the occurrence of the first lightning flash.

a. Differences in the shapes of graupel particles between thunderstorms and non-thunderstorms

The mean values of Z_H and Z_{DR} corresponding to graupel particles (the radar sample grids are identified as graupel) above the ~−3°C isotherm height (avoiding melting effects) in thunderstorms and non-thunderstorms during each stage of cloud development are displayed in Figure 5. Each orange dot indicates the mean values of Z_H and Z_{DR} corresponding to graupel above the ~−3°C isotherm height in a thunderstorm; each blue dot indicates that in a non-thunderstorm. On the basis of these results, the average intensity of the Z_{DR} corresponding to the graupel particles decreases with cloud development, which indicates that the graupel particles gradually approach a spherical shape (Figure 5d). The most remarkable indicator is that the graupel particles in the majority of the thunderstorms have lower Z_{DR} values with a mean value of ~0.3 dB when the first lightning flashes occur; however, this lower Z_{DR} value is not evident in non-thunderstorms, even during the most intense echo stage of cloud development, with a mean value of ~0.5 dB. Moreover, the Z_{DR} values approach 0 dB, corresponding to stronger Z_H values when the average intensity of the Z_H exceeds 35 dBZ. Thus, we speculated that heavily rimed graupel was present, the size increased, and the shape tended to be spherical.

Li et al. (2018) presented a quantitative relationship between the riming and shape of snow aggregates in only winter snowstorms; however, we examined the relationship in deep convection or thunderstorms in the present study. In Li et al. (2018), particles with $Z_H > 15$ dBZ, $Z_{DR} > 0.4$ dB, and above the ~−3°C isotherm height are likely to be lightly rimed (rime mass fraction ~< 0.2), and particles with $Z_H > 15$ dBZ, $-0.2 < Z_{DR} < 0.15$ dB, and above the ~−3°C isotherm height are likely to be moderately or heavily rimed (rime mass fraction ~> 0.4). The rime mass fraction is defined as the ratio of the accreted ice mass to the total ice particle mass; more details on the rime mass fraction can be found in Li et al. (2018). In Figures 5a, b, and c, the shaded area in blue indicates the high possibility that graupel particles are lightly rimed; in contrast, the shaded area in yellow indicates that the graupel particles are moderately or heavily rimed, as in Li et al. (2018). The results from Li et al. (2018) are limited to only winter snowstorms; the mechanism for

producing graupel in winter snowstorms is initiated via the aggregation of ice crystals into snow aggregates, followed by riming of the snow aggregate into graupel and possibly even small hail as the rime density increases (Heymsfield, 1982; Li et al., 2018). This process is different from the coalescence-freezing mechanism in warm-season thunderstorms, but the final shape of the graupel particles when first lightning flashes occurred in this study approached the shape of moderately or heavily rimed ice particles in Li et al. (2018).

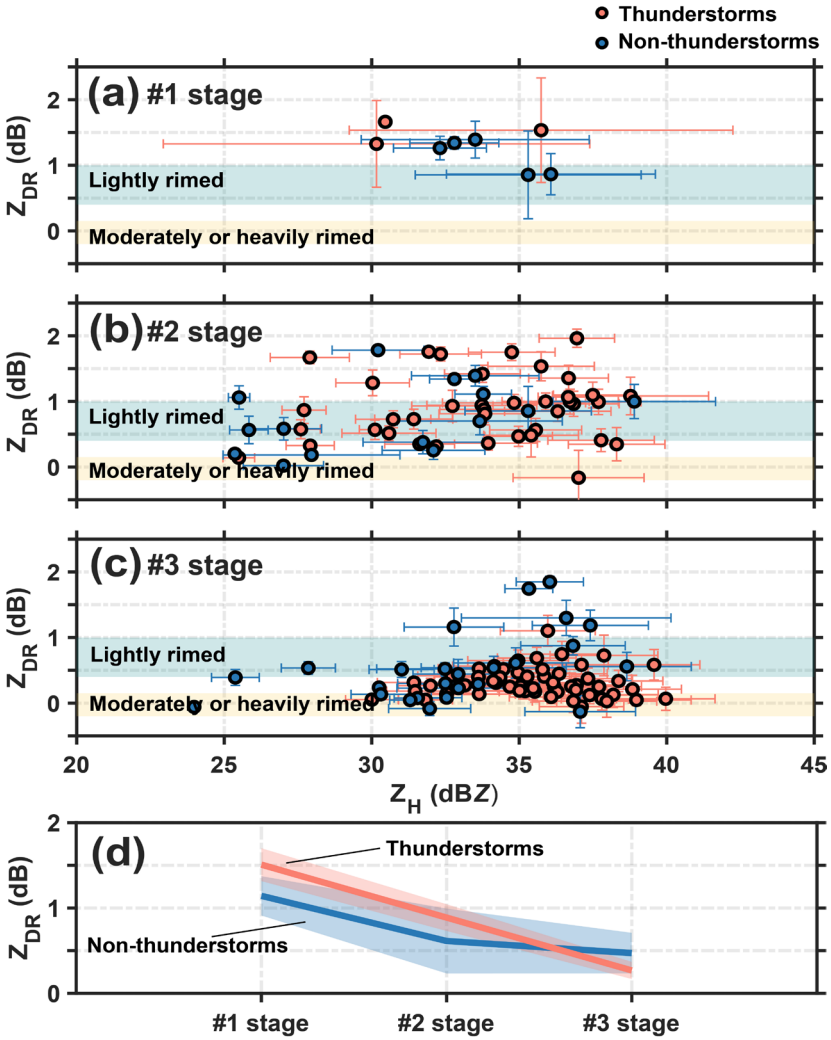

Figure 5. Graupel shape in and/or before the first lightning flash occurrence. Scatter plots with error bars for the mean values of Z_H and Z_{DR} corresponding to graupel particles above the ~−3°C isotherm height in thunderstorm (orange) and non-thunderstorm (blue) cells during each stage of cloud development. Error bars are computed as 95% confidence intervals. The inferred differences in the efficiency of the riming process are shown by the threshold values of Z_H and Z_{DR}; the shaded area in blue indicates the high possibility that graupel particles are lightly rimed, and comparatively, the shaded area in yellow indicates that graupel particles are moderately or heavily rimed. (a) First stage, (b) second stage, and (c) third stage of cloud development. In addition, the statistical mean values are given in (d), and the orange (blue) line indicates the mean value of the Z_{DR} corresponding to the above

scatters in thunderstorms (non-thunderstorms) during each stage of cloud development. The shaded area indicates the 95% confidence interval.

b. Observational characteristics associated with the source initiation and channel of the first lightning flash

The characteristics at positions with source initiation and channel characteristics of the first lightning flash are shown in Figure 6, including the height distribution, associated hydrometeor type, and values of Z_H and Z_{DR}. The heights of the initiation sources and propagation sources of the first lightning flashes determined via LFEDA are concentrated at an approximate −10°C isotherm height (Figure 6a), which is consistent with the results (i.e., the negative charge layer is located at 6 to 8 km height in thunderstorms over Guangzhou) reported by Liu et al. (2020). The hydrometeor types associated with the initiation and propagation sources are similar, and the majority of these particles are graupel and ice crystals (Figure 6b), which is understandable on the basis of the NIC electrification mechanism.

The median values of Z_H are near 31 dBZ, and the Z_{DR} values are near 0 dB (Figure 6c, d). Furthermore, Figure 7 displays the frequency of initiation and propagation sources corresponding to value intervals of Z_H (4 dBZ) and Z_{DR} (0.2 dB). The results indicate that the initiation sources of the first lightning flashes likely correspond to 20~40 dBZ and −0.2~0.4 dB (Figure 7a), and the values are likely 16~44 dBZ and −0.2~0.8 dB from propagation sources, respectively (Figure 7b).

The heights of the initiation sources and propagation sources of the first lightning flashes within isolated thunderstorms over Guangzhou are concentrated at an approximate −10°C isotherm height, which provides supplementary evidence that the main negative charge layer is located at −10°C to −20°C isotherm height on Earth, as reported by Krehbiel (1986). The values of Z_H (Z_{DR}) corresponding to the initiation sources and propagation sources of the first lightning flashes suggest that are differences in particle shape and/or size between initiation sources and propagation sources, although the differences are too subtle to quantify in this study.

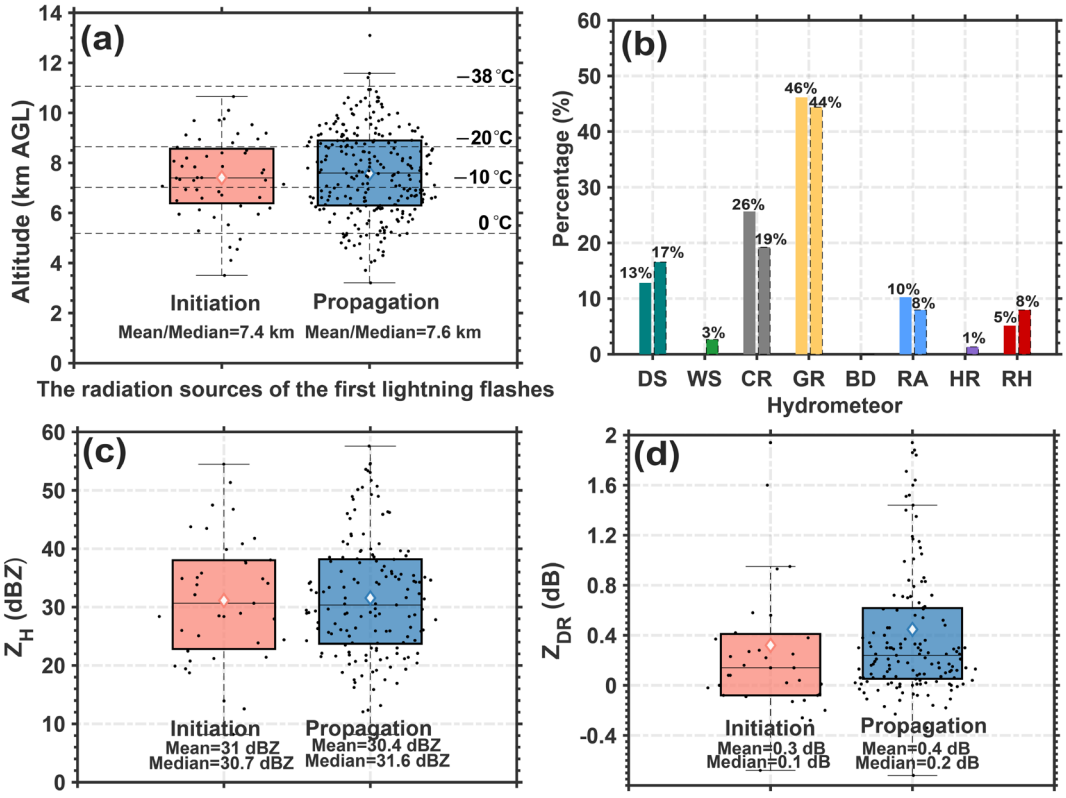

Figure 6. **The characteristics at positions with source initiation and the channel of the first lightning flash.** (a) Height distribution of the locations at the initial sources (orange box) or propagation sources (blue box) of the first lightning flashes. The 0°C, −10°C, −20°C, and −38°C isotherm heights are displayed. (b) The histogram indicates the percentage of various hydrometeors of the locations at the initial sources or propagation sources (histogram with dashed line) of the first lightning flashes. The numerical value is the percentage of various hydrometeors, such as dry snow (DS, dark green), wet snow (WS, green), crystals (CR, grey), graupel (GR, yellow), big drops (BD), raindrops (RA, blue), heavy rain (HR, purple), and rain and hail mixtures (RH, red). Radar parameters of the locations at the initial sources (orange box) or propagation sources (blue box) of the first lightning flashes: (c) horizontal reflectivity (Z_H) and (d) differential reflectivity (Z_{DR}). Each black dot indicates an individual source. The diamonds indicate the mean values.

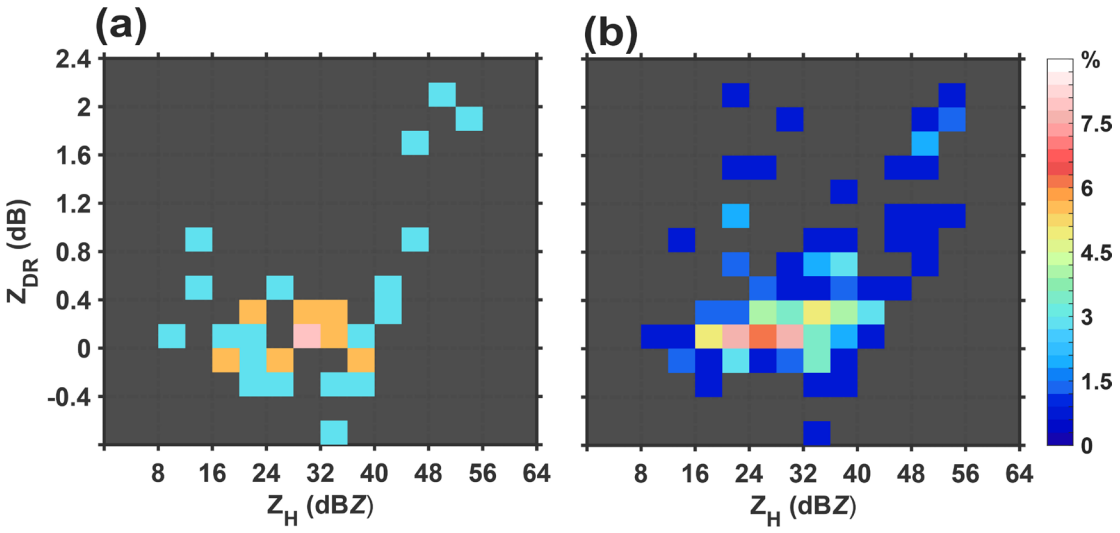

476

477 **Figure 7. The frequency of radiation sources corresponding to the value intervals of Z_H and Z_{DR}.**
478 (a) Initial sources. (b)Propagation sources.

479 *c. Signature of the Z_{DR} column*

480 Previous studies utilized Z_{DR} values ranging from 0.5–5 dB within the strong reflectivity
481 range (35–50 dBZ) above the melting layer to describe the area of the Z_{DR} column (e.g.,
482 Illingworth et al., 1987; Tuttle et al., 1989; Ryzhkov et al., 1994; Scharfenberg et al., 2005;
483 Woodard et al., 2012; Kumjian et al., 2014; Snyder et al., 2015; Zhao et al., 2020). Since the
484 development of these clouds in this study occurred during the early stage of the full evolution
485 cycle of thunderstorms, the size of the supercooled liquid water drop would not be large. Thus, we
486 used Z_{DR} values of 0.5 dB within a reflectivity range of 30 dBZ above the melting layer to
487 investigate the characteristics of the Z_{DR} column.

488 Figure 8 shows the height of the Z_{DR} column within thunderstorms or non-thunderstorms
489 during each stage of cloud development. The computation of the Z_{DR} column height is similar to
490 that in Snyder et al. (2015), and this height is the vertically continuous maximum depth of the Z_{DR}
491 column. The signature of the Z_{DR} column clearly coincides with the development of clouds
492 (Figure 8). Most thunderstorms (98.2%) displayed a deep Z_{DR} column with a mean depth of the
493 Z_{DR} column of ~2.5 km when the first lightning flash occurred; however, only 48.7% of
494 non-thunderstorms corresponded to a shallow Z_{DR} column with a mean value of ~1.1 km (Figure
495 8a, b). Moreover, 66.7% of the thunderstorms presented a deeper Z_{DR} column with a mean value
496 of ~1.5 km during the second stage of cloud development, and 30.8% of the non-thunderstorms

presented a shallower Z_{DR} column with a mean value of ~0.99 km during the second stage of cloud development (Figure 8a, b).

The results indicate that strong relationship between the Z_{DR} column and the occurrence of the first lightning flash is persistent. A deeper Z_{DR} column suggests a greater graupel volume. However, the occurrence frequency of the Z_{DR} column for non-thunderstorms is slightly greater than that for thunderstorms during the first stage of cloud development (Figure 8a, b). This phenomenon may be related to the results of Zhao et al. (2022); specifically, the Z_{DR} values below the −10°C isotherm height of non-thunderstorms were greater than those of thunderstorms within the first radar echo.

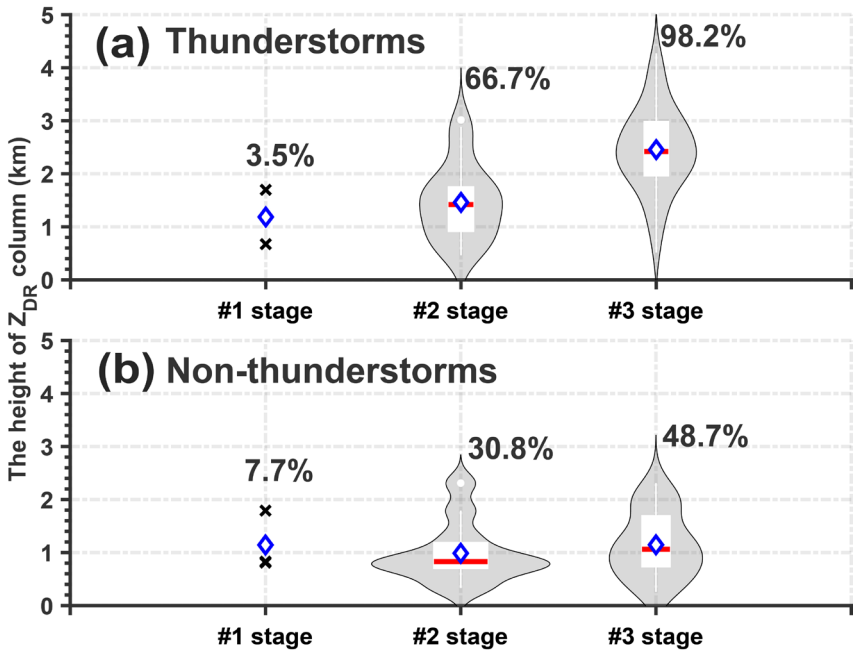

Figure 8. **Z_{DR} column information in and/or before the first lightning flash occurrence.** Violin plots of the Z_{DR} column depth of thunderstorm or non-thunderstorm cells during each stage of cloud development, showing the average (blue diamond), interquartile range (rectangle), 10th and 90th percentiles (whiskers), and kernel density estimation (gray shading). (a) Thunderstorms. (b) Non-thunderstorms. The numerical value is the percentage of thunderstorms that show the Z_{DR} column signature.

4. Summary

In this study, a combination of lightning location systems and dual-polarization radar measurements was employed to study the ice microphysics of isolated thunderstorms and non-thunderstorms in southern China during the warm season. From the unique perspective of

comparing radar signatures and inferred graupel information between isolated thunderstorm and non-thunderstorm cells during each stage of cloud development, lightning generation in clouds was found to be a good indicator of the formation of deep convective clouds. The echo intensities, echo-top heights and echo depths were greater in clouds when the first lightning flash occurred, which indicated more severe updrafts in thunderstorms than in non-thunderstorms. Moreover, a greater graupel volume was clearly observed in clouds when the first lightning flash occurred, and the maximum difference in graupel volume in the height layer between thunderstorms and non-thunderstorms reached approximately 7.6 km^3, corresponding to an approximate −10°C isotherm height.

The variation in the average Z_{DR} intensity corresponding to the graupel particles above the ~−3°C isotherm height during the three stages of cloud development indicated that graupel particles were more spherical (the mean Z_{DR} value was ~0.3 dB) and were more likely to generate lightning. The Z_{DR} values approached 0 dB, corresponding to stronger Z_H values; the average intensity of the Z_H exceeded 35 dBZ. When the first lightning flashes occurred in clouds, a decrease in the Z_{DR} value and an increase in the Z_H value of graupel were observed; these results indicate that heavily rimed ice particles were present and that the shape of these particles was similar to that of moderately or heavily rimed ice particles within winter snowstorms.

Furthermore, observational characteristics associated with the source initiation and channel of the first lightning flash were investigated. The results revealed that these sources were concentrated at an isotherm height of approximately −10°C and mainly corresponded to graupel and ice crystals. The median values of Z_H or Z_{DR} at the positions of source initiation and the channel of the first lightning flashes were nearly 31 dBZ or 0 dB. In addition, we suggest that the differences in particle shape and/or size between the initiation sources and propagation sources of the first lightning flashes persist.

Moreover, the results indicated a strong relationship between the Z_{DR} column and the occurrence of the first lightning flash; 98.2% of the clouds were equipped with a Z_{DR} column with a mean depth of ~2.5 km when the first lightning flash occurred. In addition, a deeper Z_{DR} column corresponded to a greater graupel volume. Thus, the coalescence-freezing mechanism dominated the formation of graupel within warm-season isolated thunderstorms over southern China, and the

546 results were consistent with those of previous studies (e.g., Brahams, 1986; Beard, 1992; Herzegh
547 and Jameson, 1992; Bringi et al., 1997; Smith et al., 1999; Carey and Rutledge, 2000; Stolzenburg
548 et al., 2015; Mattos et al., 2017) but increased the knowledge of the quantified characteristics of
549 the Z_{DR} column for the first lightning flash occurrence in warm-season isolated thunderstorms on
550 the basis of relatively large sample statistics (Table 1 shows details of cases in related
551 investigations for isolated thunderstorms).

References	Number of cases (thunderstorms)	Number of cases (non-thunderstorms)
Workman and Reynolds, 1949	12	×
Reynolds and Brook, 1956	5	×
Goodman et al., 1988	1	×
Ramachandran et al., 1996	2	×
Jameson et al., 1996	3	×
Woodard et al., 2012	31	19
Stolzenburg et al., 2015	3	×
Mattos et al., 2017	46	×

552 Table 1. Details of the cases in the references.

553 However, our results were obtained by comparing the characteristics of the polarimetric
554 parameters according to the graupel particles inferred via a hydrometeor identification method.
555 The inferred graupel volume was an indication that graupel could be present among other
556 hydrometeors in that volume. From the perspective of radar, the dominant particle in this volume
557 was graupel. Fortunately, we focused on comparing the graupel volume between thunderstorms
558 and non-thunderstorms; therefore, we believe that the errors in this volume resulting from other
559 secondary hydrometeors could be neutralized by comparisons with the same detected data and
560 methods.

561 In addition, unlike previous similar studies (e.g., Mattos et al., 2016, 2017), we studied the
562 microphysical differences between isolated thunderstorms and non-thunderstorms during the
563 warm season over southern China on the basis of polarimetric radar and lightning mapping array
564 instead of studying the evolution variation within the same thunderstorm (Mattos et al., 2017) or
565 studying the differences between storm vertical profiles in three-dimensional Cartesian boxes with
566 lightning and without lightning (Mattos et al., 2016).

Although the results from this study could provide a possible index or method based on polarimetric radar for warning of the first lightning flash occurrence within warm-season cell storms, understanding the microphysical characteristics and applying that in the numerical simulations would be the optimal method for providing lightning flash warnings in the future.

Acknowledgements

The authors acknowledge the Guangzhou Institute of Tropical and Marine Meteorology for collecting and archiving the radar, the surface, and the lightning observations. And authors also acknowledge the State Key Laboratory of Severe Weather, Chinese Academy of Meteorological Sciences & Laboratory of Lightning Physics and Protection Engineering for three-dimensional lightning location data. This research has been supported by the National Natural Science Foundation of China (grants 42175090, 42305079, 42305087), the China Postdoctoral Science Foundation (grant 2023M730619), the Scientific Research Fund of Chengdu University of Information Technology (grants KYTZ202213, KYQN202301, KYQN202307), the Scientific Research Fund of CAMS State Key Laboratory of Severe Weather (2021LASW-B02), and Basic Research Fund of CAMS (451490, 2023Z008).

Open Research

The sounding data is available at http://weather.uwyo.edu/upperair/sounding.html. The data in this study can be obtained from Figshare (Zhao, 2024).

References

Barthe, C., and Pinty, J.-P.: Simulation of electrified storms with comparison of the charge structure and lightning efficiency, *Journal of Geophysical Research*, 112, D19204,

doi:10.1029/2006JD008241, 2007.

Basarab, B. M., Rutledge, S. A., and Fuchs, B. R.: An improved lightning flash rate parameterization developed from Colorado DC3 thunderstorm data for use in cloud-resolving chemical transport models, *Journal of Geophysical Research: Atmospheres*, 120, 9481–9499, doi:10.1002/2015JD023470, 2015.

Beard, K. V.: Ice initiation in warm-base convective clouds: An assessment of microphysical mechanisms, *Atmospheric Research*, 28, 125–152, https://doi.org/10.1016/0169-8095(92)90024-5, 1992.

Bechini, R., and Chandrasekar, V.: A Semisupervised Robust Hydrometeor Classification Method for Dual-Polarization Radar Applications, *Journal of Atmospheric and Oceanic Technology*, 32, 22–47, https://doi.org/10.1175/JTECH-D-14-00097.1, 2015.

Braham, R. R. Jr.: The cloud physics of weather modification. Part 1: Scientific basis, *WMO Bulletin*, 35, 215–221, 1986.

Bringi, V. N., Knupp, K., Detwiler, A., Liu, L., Caylor, I. J., and Black, R. A.: Evolution of a Florida Thunderstorm during the Convection and Precipitation/Electrification Experiment: The Case of 9 August 1991, *Monthly Weather Review*, 125, 2131–2160, doi: https://doi.org/10.1175/1520-0493(1997)125<2131:EOAFTD>2.0.CO;2,1997.

Brune, W. H., McFarland, P. J., Bruning, E., Waugh, S., MacGorman, D., Miller, D. O., Jenkins, J. M., Ren, X., Mao, J., and Peischl, J.: Extreme oxidant amounts produced by lightning in storm clouds, *Science*, 372, 711–715, doi: 10.1126/science.abg0492, 2021.

Carey, L. D., and Rutledge, S. A.: The Relationship between precipitation and lightning in tropical island convection: A C-Band polarimetric radar study, *Monthly Weather Review*, 128, 2687–2710, https://doi.org/10.1175/1520-0493(2000)128<2687:TRBPAL>2.0.CO;2, 2000.

Chen, G., Zhao, K., Wen, L., Yang, J., Zheng, Y., Xu, F., Lyu, F., Sun, K., and Sun, L.: Linking ice-phase microphysics to raindrop characteristics in deep convection: A warm-sector extreme rainfall case study in Eastern China, *Earth and Space Science*, 10, e2022EA002697, https://doi.org/10.1029/2022EA002697, 2023.

Chen, L., Zhang, Y. J., Lyu, W., Zheng, D., Zhang, Y., Chen, S., and Huang, Z.: Performance evaluation for a lightning location system based on observations of artificially triggered lightning and natural lightning flashes, *Journal of Atmospheric and Oceanic Technology*, 29,

1835–1844, https://doi.org/10.1175/JTECH-D-12-00028.1, 2012.

Cui, Y., Zheng, D., Zhang, Y. J., Ruan, Z., Li, F., Yao, W., Meng, Q., and Zhao, C.: Association of lightning occurrence with precipitation cloud column structure at a fixed position, *Atmospheric Research*, 267, 105989, https://doi.org/10.1016/j.atmosres.2021.105989, 2022.

Dye, J. E., Jones, J. J., Winn, W. P., Cerni, T. A., Gardiner, B., Lamb, D., Pitter, R. L., Hallett, J., and Saunders, C. P. R.: Early electrification and precipitation development in a small, isolated Montana cumulonimbus, *Journal of Geophysical Research: Atmospheres*, 91, 1231–1247, https://doi.org/10.1029/JD091iD01p01231, 1986.

Fan, J. W., Rosenfeld, D., Zhang, Y., Giangrande, S. E., Li, Z., Machado, L. A. T., Martin, S. T., Yang, Y., Wang, J., Artaxo, P., Barbosa, H. M. J., Braga, R. C., Comstock, J. M., Feng, Z., Gao, W., Gomes, H. B., Mei, F., Pöhlker, C., Pöhlker, M. L., Pöschl, U., and de Souza, R. A. F.: Substantial convection and precipitation enhancements by ultrafine aerosol particles, *Science*, 359, 411–418, DOI: 10.1126/science.aan8461, 2018.

Fan, X., Zhang, Y. J., Zheng, D., Zhang, Y., Lyu, W., Liu, H., and Xu, L.: A new method of three-dimensional location for low-frequency electric field detection array, *Journal of Geophysical Research: Atmospheres*, 123, 8792–8812, https://doi.org/10.1029/2017JD028249, 2018.

Goodman, S. J., Buechler, D. E., Wright, P. D., and Rust, W. D.: Lightning and precipitation history of a microburst-producing storm, *Geophysical Research Letters*, 15, 1185–1188, https://doi.org/10.1029/GL015i011p01185, 1988.

Hall, M. P. M., Cherry, S. M., Goddard, J. W. F., and Kennedy, G. R.: Rain drop sizes and rainfall rate measured by dual-polarization radar, *Nature*, 285, 195–198, https://doi.org/10.1038/285195a0, 1980.

Hayashi, S., Umehara, A., Nagumo, N., and Ushio, T.: The relationship between lightning flash rate and ice-related volume derived from dual-polarization radar, *Atmospheric Research*, 248, 105166, https://doi.org/10.1016/j.atmosres.2020.105166, 2021.

Helsdon Jr., J. H., Wojcik, W. A. and Farley, R. D.: An examination of thunderstorm-charging mechanisms using a two-dimensional storm electrification model, *Journal of Geophysical Research: Atmospheres*, 106(D1), 1165–1192, doi:10.1029/2000JD900532, 2001.

Herzegh, P. H., and Jameson, A. R.: Observing Precipitation through Dual-Polarization Radar

Measurements, *Bulletin of the American Meteorological Society*, 73, 1365–1376, https://doi.org/10.1175/1520-0477(1992)073<1365:OPTDPR>2.0.CO;2, 1992.

Heymsfield, A. J.: A Comparative Study of the Rates of Development of Potential Graupel and Hail Embryos in High Plains Storms, *Journal of the Atmospheric Sciences*, 39, 2867–2897, https://doi.org/10.1175/1520-0469(1982)039<2867:ACSOTR>2.0.CO;2, 1982.

Huang, H., Zhao, K., Chan, J. C. L., and Hu, D.: Microphysical Characteristics of Extreme-Rainfall Convection over the Pearl River Delta Region, South China from Polarimetric Radar Data during the Pre-summer Rainy Season, *Advances in Atmospheric Sciences*, 40, 874–886, https://doi.org/10.1007/s00376-022-1319-8, 2023.

Hu, J., Rosenfeld, D., Ryzhkov, A., Zrnic, D., Williams, E., Zhang, P., Snyder, J. C., Zhang, R., and Weitz, R.: Polarimetric radar convective cell tracking reveals large sensitivity of cloud precipitation and electrification properties to CCN, *Journal of Geophysical Research: Atmospheres*, 124, 12194–12205, https://doi.org/10.1029/2019JD030857, 2019.

Illingworth, A. J., Goddard, J. W. F., and Cherry, S. M.: Polarization radar studies of precipitation development in convective storms, *Quarterly Journal of the Royal Meteorological Society*, 113, 469–489, https://doi.org/10.1002/qj.49711347604, 1987.

Jameson, A. R., Murphy, M. J. and Krider, E. P.: Multiple-parameter radar observations of isolated Florida thunderstorms during the onset of electrification, *Journal of Applied Meteorology and Climatology*, 35, 343–354, https://doi.org/10.1175/1520-0450(1996)035<0343:MPROOI>2.0.CO;2, 1996.

Kouketsu, T., Uyeda, H., Ohigashi, T., Oue, M., Takeuchi, H., Shinoda, T., Tsuboki, K., Kubo, M., and Muramoto, K.: A Hydrometeor Classification Method for X-Band Polarimetric Radar: Construction and Validation Focusing on Solid Hydrometeors under Moist Environments, *Journal of Atmospheric and Oceanic Technology*, 32, 2052–2074, https://doi.org/10.1175/JTECH-D-14-00124.1, 2015.

Krehbiel, P. R., Brook, M., and McCrory, R. A.: An Analysis of the Charge Structure of Lightning Discharges to Ground, *Journal of Geophysical Research*, 84, 2432–2456, doi:10.1029/JC084iC05p02432, 1979.

Kumjian, M. R.: Principles and applications of dual-polarization weather radar. Part I: Description of the polarimetric radar variables, *Journal of Operational Meteorology*, 1, 226–242,

684 doi:10.15191/nwajom.2013.0119, 2013.
685 Kumjian, M. R., Khain, A. P., Benmoshe, N., Ilotoviz, E., Ryzhkov, A. V., and Phillips, V. T. J.:
686 The anatomy and physics of ZDR columns: Investigating a polarimetric radar signature with
687 a spectral bin microphysical model, *Journal of Applied Meteorology and Climatology*, 53,
688 1820–1843, https://doi.org/10.1175/JAMC-D-13-0354.1, 2014.
689 Kumjian, M. R., and Ryzhkov, A. V.: Polarimetric signatures in supercell thunderstorms, *Journal*
690 *of Applied Meteorology and Climatology*, 47, 1940–1961,
691 https://doi.org/10.1175/2007JAMC1874.1, 2008.
692 Laksen, H. R., and Stansbury, E. J.: Association of lightning flashes with precipitation cores
693 extending to height 7 km, *Journal of Atmospheric and Terrestrial Physics*, 36, 1547–1548,
694 https://doi.org/10.1016/0021-9169(74)90232-3, 1974.
695 Lang, T. J., and Rutledge, S. A.: A Framework for the Statistical Analysis of Large Radar and
696 Lightning Datasets: Results from STEPS 2000, *Monthly Weather Review*, 139, 2536–2551,
697 https://doi.org/10.1175/MWR-D-10-05000.1, 2011.
698 Latham, J.: The electrification of thunderstorms, *Quarterly Journal of the Royal Meteorological*
699 *Society*, 107, 277–298, https://doi.org/10.1002/qj.49710745202, 1981.
700 Latham, J., Petersen, W. A., Deierling, W. and Christian, H. J.: Field identification of a unique
701 globally dominant mechanism of thunderstorm electrification, *Quarterly Journal of the Royal*
702 *Meteorological Society*, 133, 1453–1457, https://doi.org/10.1002/qj.133, 2007.
703 Li, H., Moisseev, D., and von Lerber, A.: How does riming affect dual-polarization radar
704 observations and snowflake shape? *Journal of Geophysical Research: Atmospheres*, 123,
705 6070–6081, https://doi.org/10.1029/2017JD028186, 2018.
706 Liu, Z., Zheng, D., Guo, F., Zhang, Y., Zhang, Y. J., Wu, C., Chen, H., Han, S.: Lightning activity
707 and its associations with cloud structures in a rainstorm dominated by warm precipitation,
708 *Atmospheric Research*, 246, 105120, https://doi.org/10.1016/j.atmosres.2020.105120, 2020.
709 Lyu, W., Zheng, D., Zhang, Y., Yao, W., Jiang, R., Yuan, S., Liu, D., Lyu, F., Zhu, B., Lu, G.,
710 Zhang, Q., Tan, Y., Wang, X., Liu, Y., Chen, S., Chen, L., Li, Q., and Zhang, Y. J.: A Review
711 of Atmospheric Electricity Research in China from 2019 to 2022, *Advances in Atmospheric*
712 *Sciences*, 40, 1457–1484, https://doi.org/10.1007/s00376-023-2280-x, 2023.
713 MacGorman, D. R., and Rust, W. D.: The electrical nature of storms, *Oxford University Press*, 422

pp., 1998.

Mai, C., and Du, Y.: Mesoscale moisture transport in determining the location of daytime convection initiations clustered in time and space over southern China, *Journal of Geophysical Research: Atmospheres*, 127, e2021JD036098, https://doi.org/10.1029/2021JD036098, 2022.

Mansell, E. R., MacGorman, D. R., Ziegler, C. L., and Straka, J. M.: Charge structure and lightning sensitivity in a simulated multicell thunderstorm, *Journal of Geophysical Research: Atmospheres*, 110, D12101, doi:10.1029/2004JD005287, 2005.

Marshall, J. S., and Radhakant, S.: Radar Precipitation Maps as Lightning Indicators, *Journal of Applied Meteorology and Climatology*, 17, 206–212, https://doi.org/10.1175/1520-0450(1978)017<0206:RPMALI>2.0.CO;2, 1978.

Mather, G. K., Morrison, B. J., and Morgan, G. M.: A Preliminary Assessment of the Importance of Coalescence in Convective Clouds of the Eastern Transvaal, *Journal of Applied Meteorology and Climatology*, 25, 1780–1784, https://doi.org/10.1175/1520-0450(1986)025<1780:APAOTI>2.0.CO;2, 1986.

Mattos, E. V., Machado, L. A. T., Williams, E. R., and Albrecht, R. I.: Polarimetric radar characteristics of storms with and without lightning activity, *Journal of Geophysical Research: Atmospheres*, 121, 14201–14220, https://doi.org/10.1002/2016JD025142, 2016.

Mattos, E. V., Machado, L. A. T., Williams, E. R., Goodman, S. J., Blakeslee, R. J., and Bailey, J. C.: Electrification life cycle of incipient thunderstorms, *Journal of Geophysical Research: Atmospheres*, 122, 4670–4697, https://doi.org/10.1002/2016JD025772, 2017.

Park, H. S., Ryzhkov, A. V., Zrnić, D. S., and Kim, K.: The Hydrometeor Classification Algorithm for the Polarimetric WSR-88D: Description and Application to an MCS, *Weather and Forecasting*, 24, 730–748, https://doi.org/10.1175/2008WAF2222205.1, 2009.

Pickering, K. E., Bucsela, E., Allen, D., Ring, A., Holzworth, R., and Krotkov, N.: Estimates of lightning NO_x production based on OMI NO_2 observations over the Gulf of Mexico, *Journal of Geophysical Research: Atmospheres*, 121, 8668–8691, https://doi.org/10.1002/2015JD024179, 2016.

Qie, X., Yuan, S., Chen, Z., Wang, D., Liu D., Sun, M., Sun, Z., Srivastava, A., Zhang, H., Lu, J., Xiao, H., Bi, Y., Feng, L., Tian, Y., Xu, Y., Jiang, R., Liu, M., Xiao, X., Duan, S., Su, D., Sun,

744 C., Xu, W., Zhang, Y., Lu, G., Zhang, D., Yin, Y., and Yu, Y.: Understanding the
745 dynamical-microphysical-electrical processes associated with severe thunderstorms over the
746 Beijing metropolitan region, *Science China Earth Sciences*, 64, 10–26.
747 https://doi.org/10.1007/s11430-020-9656-8, 2021.
748 Ramachandran, R., Detwiler, A., Helsdon, J., Smith, P. L., and Bringi, V. N.: Precipitation
749 development and electrification in Florida thunderstorm cells during Convection and
750 Precipitation/Electrification Project, *Journal of Geophysical Research: Atmospheres*, 101,
751 1599–1619, https://doi.org/10.1029/95JD02931, 1996.
752 Reynolds, S. E., and Brook, M.: CORRELATION OF THE INITIAL ELECTRIC FIELD AND
753 THE RADAR ECHO IN THUNDERSTORMS, *Journal of the Atmospheric Sciences*, 13,
754 376–380, https://doi.org/10.1175/1520-0469(1956)013<0376:COTIEF>2.0.CO;2, 1956.
755 Reynolds, S. E., Brook, M., and Gourley, M. F.: Thunderstorm charge separation, *Journal of the*
756 *Atmospheric Sciences*, 14, 426–436,
757 https://doi.org/10.1175/1520-0469(1957)014<0426:TCS>2.0.CO;2, 1957.
758 Rosenfeld, D.: TRMM observed first direct evidence of smoke from forest fires inhibiting rainfall,
759 *Geophysical Research Letters*, 26, 3105–3108, https://doi.org/10.1029/1999GL006066, 1999.
760 Rosenfeld, D., Lohmann, U., Raga, G. B., O'Dowd, C. D., Kulmala, M., Fuzzi, S., Reissell, A.,
761 and Andreae, M. O.: Flood or drought: How do aerosols affect precipitation? *Science*, 321,
762 1309–1313, doi:10.1126/science.1160606, 2008.
763 Ryzhkov, A. V., Zhuravlyov, V. B., and Rybakova, N. A.: Preliminary results of X-band
764 polarization radar studies of clouds and precipitation, *Journal of Atmospheric and Oceanic*
765 *Technology*, 11, 132–139,
766 https://doi.org/10.1175/1520-0426(1994)011<0132:PROXBP>2.0.CO;2, 1994.
767 Saunders, C.: Charge Separation Mechanisms in Clouds, *Space Science Reviews*, 137, 335–353,
768 https://doi.org/10.1007/s11214-008-9345-0, 2008.
769 Saunders, C. P. R., Keith, W. D., and Mitzeva, R. P.: The effect of liquid water on thunderstorm
770 charging, *Journal of Geophysical Research*, 96, 11007–11017,
771 https://doi.org/10.1029/91JD00970, 1991.
772 Scharfenberg, K. A., Miller, D. J., Schuur, T. J., Schlatter, P. T., Giangrande, S. E., Melnikov, V. M.,
773 Burgess, D. W., Andra, D. L., Foster, M. P. Jr., and Krause, J. M.: The Joint Polarization

774 Experiment: Polarimetric Radar in Forecasting and Warning Decision Making, *Weather and*
775 *Forecasting*, 20, 775–788, https://doi.org/10.1175/WAF881.1, 2005.
776 Seliga, T. A., and Bringi, V. N.: Potential Use of Radar Differential Reflectivity Measurements at
777 Orthogonal Polarizations for Measuring Precipitation, *Journal of Applied Meteorology and*
778 *Climatology*, 15, 69–76,
779 https://doi.org/10.1175/1520-0450(1976)015<0069:PUORDR>2.0.CO;2, 1976.
780 Shi, D., Zheng, D., Zhang, Y., Zhang, Y. J., Huang, Z., and Lyu, W.: Low-frequency E-field
781 Detection Array (LFEDA)-Construction and preliminary results, *Science China Earth*
782 *Sciences*, 60, 1896–1908, https://doi.org/10.1007/s11430-016-9093-9, 2017.
783 Smith, P. L., Musil, D. J., Detwiler, A. G., and Ramachandran, R.: Observations of Mixed-Phase
784 Precipitation within a CaPE Thunderstorm, *Journal of Applied Meteorology and Climatology*,
785 38, 145–155, https://doi.org/10.1175/1520-0450(1999)038<0145:OOMPPW>2.0.CO;2,
786 1999.
787 Snyder, J. C., Ryzhkov, A. V., Kumjian, M. R., Khain, A. P., and Picca, J. C.: A ZDR column
788 detection algorithm to examine convective storm updrafts, *Weather and Forecasting*, 30,
789 1819–1844, https://doi.org/10.1175/WAF-D-15-0068.1, 2015.
790 Stolzenburg, M., Marshall, T. C., and Krehbiel, P. R.: Initial electrification to the first lightning
791 flash in New Mexico thunderstorms, *Journal of Geophysical Research: Atmospheres*, 120,
792 11,253–11,276, https://doi.org/10.1002/2015JD023988, 2015.
793 Stolzenburg, M., Marshall, T. C., and Rust, W. D.: Serial sounding of electric field through a
794 mesoscale convective system, *Journal of Geophysical Research: Atmospheres*, 106,
795 12371–12380, https://doi.org/10.1029/2001JD900074, 2001.
796 Stough, S. M., and Carey, L. D.: Observations of anomalous charge structures in supercell
797 thunderstorms in the Southeastern United States, *Journal of Geophysical Research:*
798 *Atmospheres*, 125, e2020JD033012, https://doi.org/10.1029/2020JD033012, 2020.
799 Stough, S. M., Carey, L. D., Schultz, C. J., and Cecil, D. J.: Examining conditions supporting the
800 development of anomalous charge structures in supercell thunderstorms in the Southeastern
801 United States, *Journal of Geophysical Research: Atmospheres*, 126, e2021JD034582,
802 https://doi.org/10.1029/2021JD034582, 2021.
803 Takahashi, T.: Riming electrification as a charge generation mechanism in thunderstorms, *Journal*

804 *of the Atmospheric Sciences*, 35, 1536–1548,
805 https://doi.org/10.1175/1520-0469(1978)035<1536:REAACG>2.0.CO;2, 1978.
806 Takahashi, T., Tajiri, T., and Sonoi, Y.: Charges on Graupel and Snow Crystals and the Electrical
807 Structure of Winter Thunderstorms, *Journal of the Atmospheric Sciences*, 56, 1561–1578,
808 https://doi.org/10.1175/1520-0469(1999)056<1561:COGASC>2.0.CO;2, 1999.
809 Takahashi, T., Sugimoto, S., Kawano, T., and Suzuki, K.: Riming Electrification in Hokuriku
810 Winter Clouds and Comparison with Laboratory Observations, *Journal of the Atmospheric*
811 *Sciences*, 74, 431–447, https://doi.org/10.1175/JAS-D-16-0154.1, 2017.
812 Takahashi, T., Sugimoto, S., Kawano, T., and Suzuki, K.: Microphysical structure and lightning
813 initiation in Hokuriku winter clouds, *Journal of Geophysical Research: Atmospheres*, 124,
814 13156–13181, https://doi.org/10.1029/2018JD030227, 2019.
815 Tuttle, J. D., Bringi, V. N., Orville, H. D., and Kopp, F. J.: Multiparameter radar study of a
816 microburst: Comparison with model results, *Journal of the Atmospheric Sciences*, 46,
817 601–620, https://doi.org/10.1175/1520-0469(1989)046<0601:MRSOAM>2.0.CO;2, 1989.
818 Uman, M. A., and Krider, E. P.: Natural and artificially initiated lightning, *Science*, 246, 457–464,
819 doi:10.1126/science.246.4929.457, 1989.
820 Vincent, B. R., Carey, L. D., Schneider, D., Keeter, K., and Gonski, R.: Using WSR-88D
821 reflectivity data for the prediction of cloud-to-ground lightning: A central North Carolina
822 study, *National Weather Digest*, 27, 35–44, 2003.
823 Woodard, C. J., Carey, L. D., Petersen, W. A., and Roeder, W. P.: Operational utility of
824 dual-polarization variables in lightning initiation forecasting, *Electronic J. Operational*
825 *Meteor.*, 13, 79–102, 2012.
826 Workman, E. J., and Reynolds, S. E.: Electrical activity as related to thunderstorm cell growth,
827 *Bulletin of the American Meteorological Society*, 30, 142–149,
828 https://doi.org/10.1175/1520-0477-30.4.142, 1949.
829 Wu, C., Liu, L., Wei, M., Xi, B., and Yu, M.: Statistics-based optimization of the polarimetric
830 radar hydrometeor classification algorithm and its application for a squall line in South China,
831 *Advances in Atmospheric sciences*, 35, 296–316, https://doi.org/10.1007/s00376-017-6241-0,
832 2018.
833 Zhang, Y., Lyu, W., Chen, S., Zheng, D., Zhang, Y., Yan, X., Chen, L., Dong, W., Dan, J., and Pan,

H.: A review of advances in lightning observations during the past decade in Guangdong, China, *Journal of Meteorological Research*, 30, 800–819, https://doi.org/10.1007/s13351-016-6928-7, 2016.

Zhang, Y. J., Yan, M., Sun, A., and Guo, F.: Thunderstorm electricity. *China Meteorological Press*, 384 pp., 2009.

Zhang, Y. J., Sun, A., Yan, M., Guo, F., Qie, X., and Huang, M.: Numerical Simulations of the Effects of Electric Environment on Hail Growth, *Chinese Journal of Geophysics*, 47, 29–37, https://doi.org/10.1002/cjg2.451, 2004.

Zhao, C.: Data for "On the ice microphysics of isolated thunderstorms and non-thunderstorms in southern China: A radar polarimetric perspective". Figshare. [Dataset]. https://doi.org/10.6084/m9.figshare.22718437.v6, 2024.

Zhao, C., Zhang, Y. J., Zheng, D., Liu, X., Zhang, Y., Fan, X., Yao, W., and Zhang, W.: Using polarimetric radar observations to characterize first echoes of thunderstorms and nonthunderstorms: A comparative study, *Journal of Geophysical Research: Atmospheres*, 127, e2022JD036671, https://doi.org/10.1029/2022JD036671, 2022.

Zhao, C., Zhang, Y. J., Zheng, D., Zhou, Y., Xiao, H., and Zhang, X.: An improved hydrometeor identification method for X-band dual-polarization radar and its application for one summer Hailstorm over Northern China, *Atmospheric Research*, 245, 105075, https://doi.org/10.1016/j.atmosres.2020.105075, 2020.

Zhao, C., Zheng, D., Zhang, Y. J., Liu, X., Zhang, Y., Yao, W., and Zhang, W.: Turbulence Characteristics before the Occurrence of the First Flash in Thunderstorms and Non-Thunderstorms, *Geophysical Research Letters*, 48, e2021GL094821, https://doi.org/10.1029/2021GL094821, 2021a.

Zhao, C., Zheng, D., Zhang, Y. J., Liu, X., Zhang, Y., Yao, W., and Zhang, W.: Characteristics of cloud microphysics at positions with flash initiations and channels in convection and stratiform areas of two squall lines, *Journal of Tropical Meteorology*, 37, 358–369, doi:10.16032/j.issn.1004-4965.2021.035, 2021b.

Zheng, D., Zhang, Y., Zhang, Y., Lyu, W., Chen, L., and Shi, D.: Lightning activity characteristics as indicated by lightning location systems in Guangdong, *in: 1st International Workshop of the Southern China Monsoon Rainfall Experiment (SCMREX), Beijing, China*, 12–13 April,

2017.

Zipser, E. J., Cecil, D. J., Liu, C., Nesbitt, S. W. and Yorty, D. P.: WHERE ARE THE MOST INTENSE THUNDERSTORMS ON EARTH? *Bulletin of the American Meteorological Society*, 87, 1057–1072, https://doi.org/10.1175/BAMS-87-8-1057, 2006.

Zrnic, D. S., and Ryzhkov, A. V.: Polarimetry for Weather Surveillance Radars, *Bulletin of the American Meteorological Society*, 80, 389–406, https://doi.org/10.1175/1520-0477(1999)080<0389:PFWSR>2.0.CO;2, 1999.

Authors contributions

Conceptualization: C. Zhao, Y. Zhang

Data curation: C. Zhao, Y. Zhang, D. Zheng, S. Du, and X. Liu

Formal analysis: C. Zhao, Y. Zhang, H. Li, X. Peng, P. Zhao, J. Zheng, and J. Shi

Funding acquisition: Y. Zhang, C. Zhao

Investigation: C. Zhao, Y. Zhang

Methodology: C. Zhao, Y. Zhang, and H. Li

Project Administration: Y. Zhang

Resources: C. Zhao, Y. Zhang

Software: C. Zhao, D. Zheng

Supervision: Y. Zhang

Validation: C. Zhao, Y. Zhang

Visualization: C. Zhao, Y. Zhang, and H. Li

Writing-original draft: C. Zhao, Y. Zhang, X. Peng, and H. Li

Competing interests

The contact author has declared that none of the authors has any competing interests.